DOI: 10.21062/mft.2024.025  http://www.journalmt.com

# Microstructure and Properties of Natural Alloy Prepared by Aluminothermic Reduction of Deep-Sea Nodules and Processed by Rapid Solidification

Alena Michalcová (0000-0002-1225-5380), Matouš Orlíček (0000-0003-3154-4687), Pavel Novák (0000-0001-9947-2566)
Department of Metals and Corrosion Engineering, University of Chemistry and Technology in Prague. Technická 5, 166 28 Prague 6. Czech Republic. E-mail: michalca@vscht.cz, orlicekm@seznam.cz, panovak@vscht.cz

**This paper explores the investigation of a natural alloy processed using the rapid solidification technique. The study involves the reduction of manganese nodules through aluminothermy with a 20 wt. % excess of aluminum, followed by further processing of the resulting alloy using the melt-spinning process. The obtained melt-spun ribbons were subjected to a comprehensive analysis, including X-ray diffraction, scanning electron microscopy for microstructure observation, and EDS analysis for local chemical composition. The research unveiled that the rapidly solidified ribbons consist of several key phases, including β-Mn, the Heusler phase $Mn_2FeSi$, and an intermetallic phase $(Cu,Mn)_3(Al,Si)$. Importantly, the phase composition exhibited notable differences from that of the as-reduced alloy, with a reduced number of phases in the rapidly solidified ribbons. Notably, the phase composition remained stable even after annealing, demonstrating the robustness of the rapidly solidified material. Impressively, the material exhibited a remarkable hardness of approximately 800 HV 0.1, even after 100 hours of annealing at temperatures of 500 and 750°C.**

**Keywords:** Manganese Alloy, Manganese Nodules, Natural Alloy, Rapid Solidification, Melt-spinning

## 1 Introduction

Searching for new sources of structural materials is a current problem. One of the options to solve it is utilization of materials based on deep-sea nodules. The deep-sea manganese nodules are common sediments covering the seabed. The manganese nodules are composed of oxides and hydroxides of Mn, Fe, Cu, Co, Ni, and other elements. They are typical for their black colour, size of around 5 cm, and mamillated shape (roundish with small humps) [1]. The processing of the deep-sea nodules can be divided into two main categories— hydrometallurgical and pyrometallurgical methods [2,3]. The second mentioned are in scope of this article with focus on reduction the whole nodules to achieve so called natural alloy. The reduction can be performed by different reducing agents, such as aluminium [4,5] or silicon [6]. The main problem of Mn-based materials is the fragility of α-Mn and β-Mn [7]. On the other hand, the γ-Mn has sufficient mechanical properties for utilization as structural material [7]. It was proven that addition of Al and C can stabilize the γ-Mn [7]. It was re-ported that addition of Cu and Ni also enhance stability of γ-Mn [8]. Other sources state that 5 % of elements such as C, Fe, Ni, Cu, Pd or Au is sufficient to stabilize γ-Mn to the room temperature [9,10]. It was also described that melt spinning process increases the probability of γ-Mn phase, while it is created by rapid cooling from temperatures above 1100 °C [9,10]. The natural alloy prepared by aluminothermic reduction of manganese deep-sea nodules combines the above-mentioned factors (presence of Fe, Cu and Ni and increased content of Al when excess to stoichiometry is used). This article describes microstructure and properties of this natural alloy processed by melt-spinning technique.

## 2 Experimental

The manganese nodules from the Clarion–Clipperton zone were reduced by 20 wt. % excess to a stoichiometric amount of Al. Detailed information on the reduction process is given in [4]. The reduced material was re-melted and processed by melt-spinning process with circumferential speed of 40 m/s. The ribbons achieve thickness of 40 – 50 μm and length of several centimetres. The chemical composition was measured by a fluorescence spectrometer (XRF, Axios, PANanalytical, Almelo, The Netherlands). Phase composition was determined by an X-ray diffractometer (XRD, PANanalytical X'pert PRO, Almelo, The Netherlands) with Co anode, using a step of 0.026° 2 Th. and the measuring time per step of 1 s. The materials were examined by an Olympus PME 3 (Olympus, Tokyo, Japan) light optical microscope (LOM) and a TESCAN VEGA 3 LMU scanning electron microscope (SEM, TESCAN, Brno, Czech Republic), with an accelerating voltage

of 20 kV and a working distance of 15 mm for energy dispersive spectroscopic analysis (EDS, Oxford Instruments, Abingdon, UK). Backscattered electrons (BSEs) were used for imaging. The samples were observed after etching in the 0.5% solution of HF for 3 s. The TEM observation was performed by Jeol 2200 FS equipped (TEM, Jeol, Tokyo, Japan) by EDS analyzer by Oxford Instruments (EDS, Oxford Instruments, Abingdon, UK). The Vickers microhardness (136-degree diamond pyramid indenter) was measured using a Future-Tech FM-700 device (Future-Tech Corp, Tokyo, Japan) with a load of 0.1 kg and a dwell time of 15 s. The presented value is an average of 10 measurements.

The materials were annealed at 500 °C and 750 °C for 1, 10 and 100 h and at 1000 °C for 1 and 5 h in a resistance furnace (Martinek) in evacuated ampules with subsequent air cooling. The ampules contained inert $SiO_2$ fibres to protect the light-weight ribbon from being removed during evacuation.

## 3 Results and Discussion

The melt-spinning process produces material in form of thin ribbons. The cooling speed of both sides of the ribbon differ. The highest cooling speed is achieved when the material is in direct contact with cooling wheel. This side of ribbon is labelled as the wheel side. Opposite side which was not in direct contact with cooling wheel is labelled as free side. The comparison of chemical composition of as-reduced material [4], wheel side and free side of the ribbon is given in Tab. 1.

***Tab. 1*** *Chemical composition of studied materials given in wt % (X-ray fluorescence spectrometer (XRF)); RS = rapid solidification*

| Element/Sample | As-reduced [4] | RS - wheel side | RS - free side |
|---|---|---|---|
| Mn | 57.708 | 56.003 | 57.19 |
| Al | 9.312 | 1.325 | 1.786 |
| Si | 8.001 | 7.578 | 7.283 |
| P | 0.487 | 0.519 | 0.361 |
| S | 0.118 | 0 | 0 |
| V | 0.236 | 0.195 | 0.246 |
| Fe | 15.361 | 21.217 | 20.351 |
| Co | 0.545 | 0.451 | 0.539 |
| Ni | 4.083 | 6.562 | 6.422 |
| Cu | 3.935 | 5.864 | 5.494 |
| Mo | 0.214 | 0.287 | 0.329 |

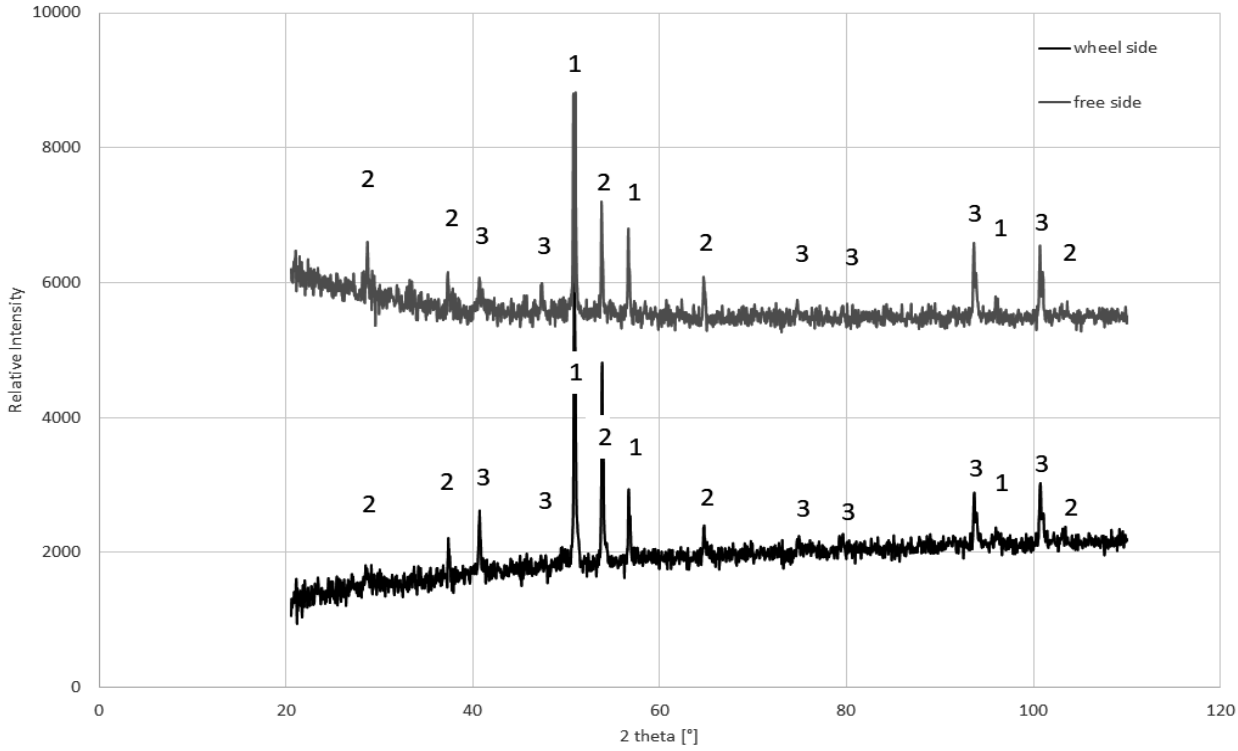


***Fig. 1*** *XRD pattern of the rapidly solidified ribbons consisting of phases: 1) β-Mn, 2) Mn2FeSi, 3) (Cu,Mn)3(Al,Si)*

The wheel side and free side exhibit similar chemical composition taking in account experimental error and natural fluctuation of chemical composition. Composition of both side of rapidly solidified ribbon slightly differs from chemical composition of the as-reduced material. The Al and S from the as-reduced material probably oxidized during remelting in the induction furnace prior melt-spinning process and were trapped in the nozzle.

Rapid solidification led to reduction of number of present phases in the system. The as-reduced alloy composed of $Mn_5Si_3$, α-Mn, $Mn_2FeAl$, $Mn_2FeSi$, $Mn_2P$, $(Cu,Mn)_3(Al,Si)$ and $Mn_3(Al,Si)$ [4]. On the hand both sides of the rapidly solidified ribbon exhibited presence only of β-Mn, $Mn_2FeSi$ and $(Cu,Mn)_3(Al,Si)$, see Fig. 1. Which means that the allying elements formed supersaturation in these detected phases. The presence of β-Mn is expectable, as this modification is created at higher cooling rates. It also seems that the cooling rates were not sufficient for forming of the intended γ-Mn phase.

The microstructure of the rapidly solidified ribbon is shown in Fig. 2. The wheel side is located at the top of the image. The microstructure does not exhibit any structure gradient caused by different cooling rates at the cross-section of the ribbon. Two phases might be distinguished in the image, but the microstructure is too fine to be analyzed by SEM-EDS.

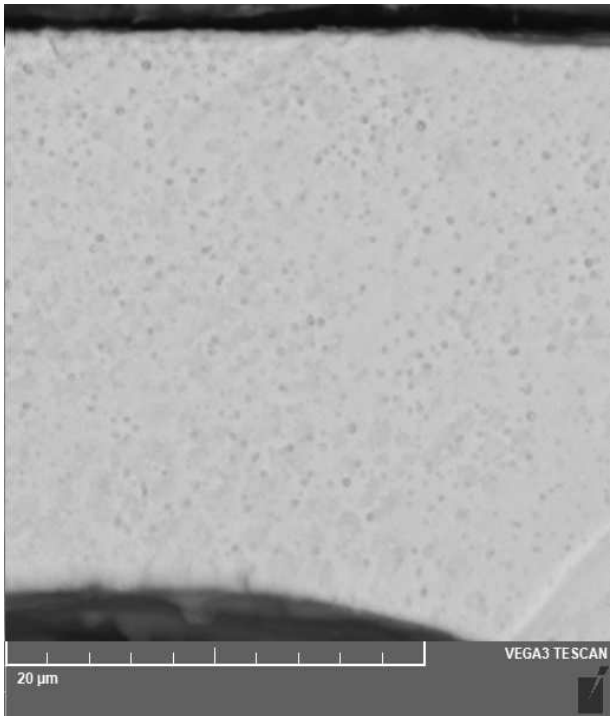


***Fig. 2*** *Microstructure of the rapidly solidified ribbon (SEM)*

The microstructure of the rapidly solidified ribbon was in detail studied by TEM. Micrographs in Fig. 3 show two distinguishable areas that belong to β-Mn and $Mn_2FeSi$ phases.

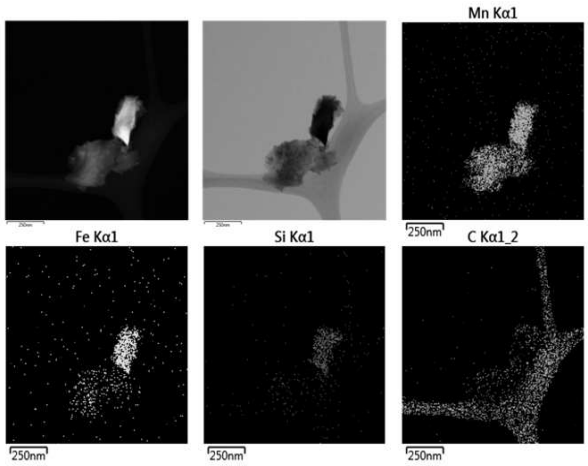


***Fig. 3*** *Microstructure of the rapidly solidified ribbon (TEM) proving presence of β-Mn and $Mn_2FeSi$ phases*

The presence of $(Cu,Mn)_3(Al,Si)$ was verified in the $Mn_2FeSi$ where it was dispersed in for of small round objects, as illustrated in Fig. 4. The system of natural alloy is very complex, so it cannot be described by existing phase diagrams. It can be only stated that this morphology is typical for cross-section of eutectic lamellas and that the presence of eutectic transformation in Heusler phases was already described [11].

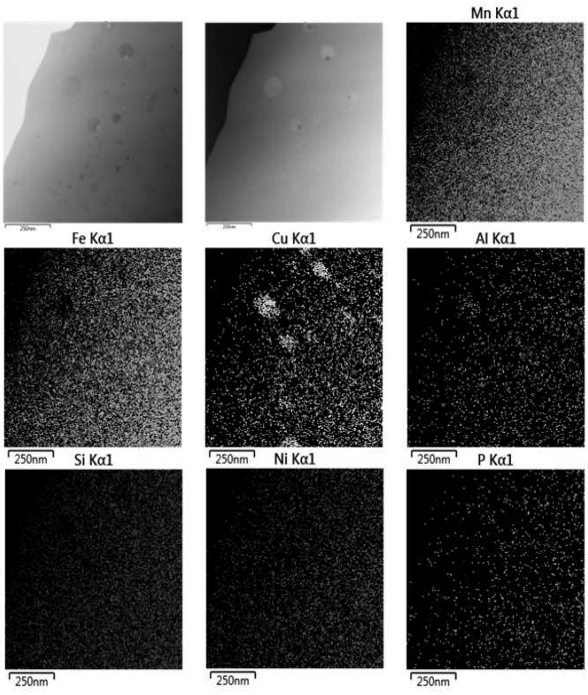


***Fig. 4*** *Microstructure of the rapidly solidified ribbon (TEM) showing $(Cu,Mn)_3(Al,Si)$ particles in $Mn_2FeSi$ matrix*

To prove the thermal stability of rapidly solidified ribbons composed of supersaturated phases, the ribbons were annealed at 500, 750 and 1000 °C. The phase composition after one hour of annealing at each temperature is shown in Fig. 5.

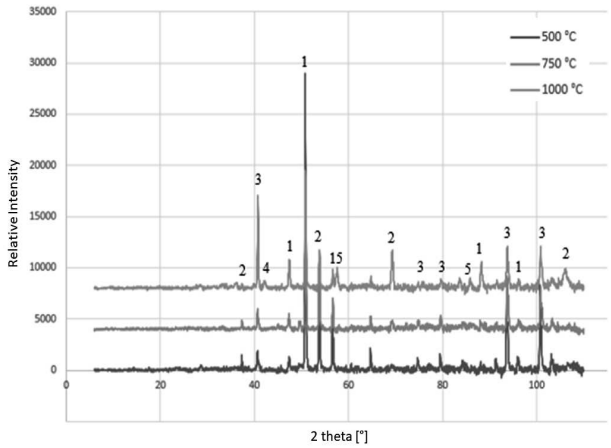


***Fig. 5*** *XRD pattern of the ribbons annealed for 1 h at various temperatures, consisting of phases : 1) β-Mn, 2) $Mn_2FeSi$, 3) $(Cu,Mn)_3(Al,Si)$ 4) $SiO_2$, 5) $Mn_2SiO_4$*

The only important change in phase composition happened at 1000 °C, where the chemical reaction (1) between ribbons and protective $SiO_2$ took place:

$$2MnO + SiO_2 \rightarrow Mn_2SiO_4 \quad (1)$$

The microstructure of ribbon annealed at 500 °C for 1 h is shown in Fig. 6. The increased amount of the $(Cu,Mn)_3(Al,Si)$ can be observed in form of bright dots in the microstructure.

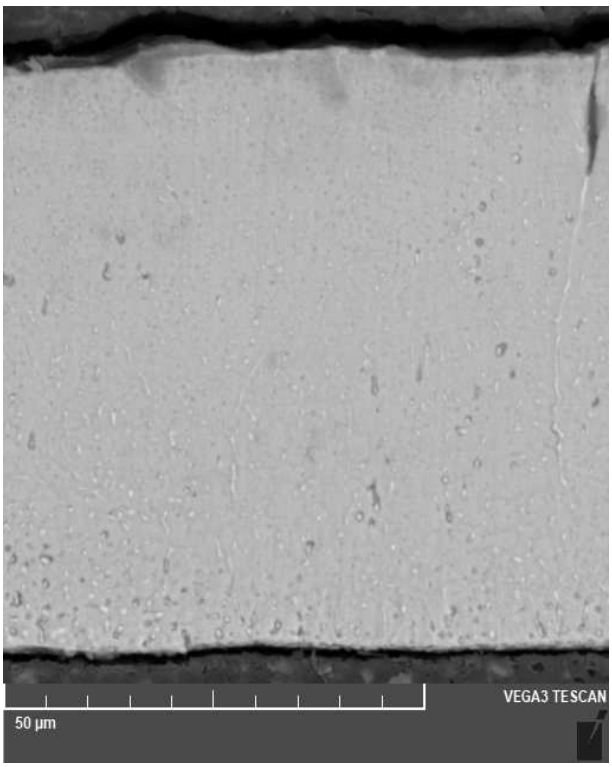


***Fig. 6*** *Microstructure of the ribbon annealed at 500 °C for 1 h (SEM)*

The microstructure of ribbon annealed at 750 °C for 1 h is shown in Fig. 7. The microstructural changes are comparable to those that happened at 500 °C.

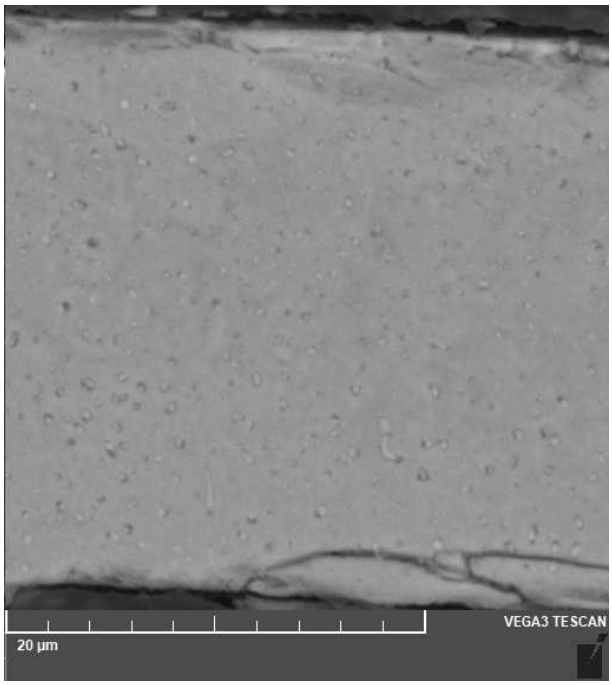


***Fig. 7*** *Microstructure of the ribbon annealed at 750 °C for 1 h (SEM)*

The microstructure of ribbon annealed at 1000 °C for 1 h is shown in Fig. 8. The amount of the $(Cu,Mn)_3(Al,Si)$ phase is significantly higher and oriented along the cross-section of the ribbon. The ribbon is covered by the oxide shell that was also detected by XRD and their presence is shown in Fig. 5.

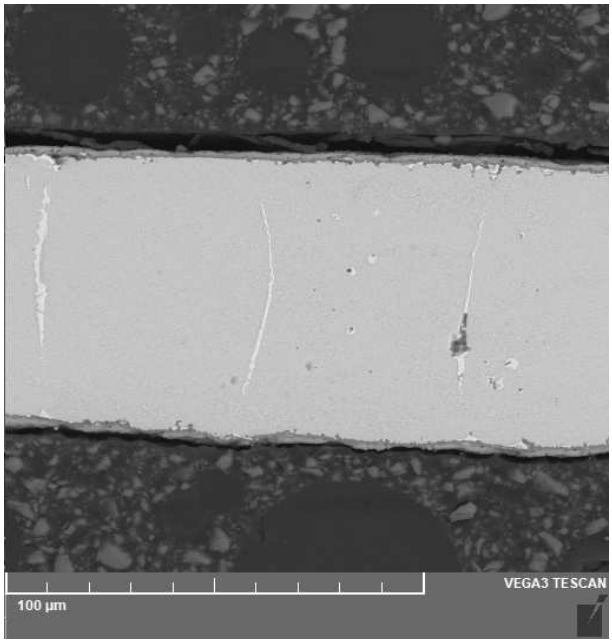


***Fig. 8*** *Microstructure of the ribbon annealed at 1000 °C for 1 h (SEM)*

Due to occurring the chemical reaction at 1000 °C, the ribbons were annealed for longer times only at temperatures of 500 and 750 °C. At these

temperatures, no change of chemical composition was observed even after 100 h of annealing, as documented in Fig. 9.

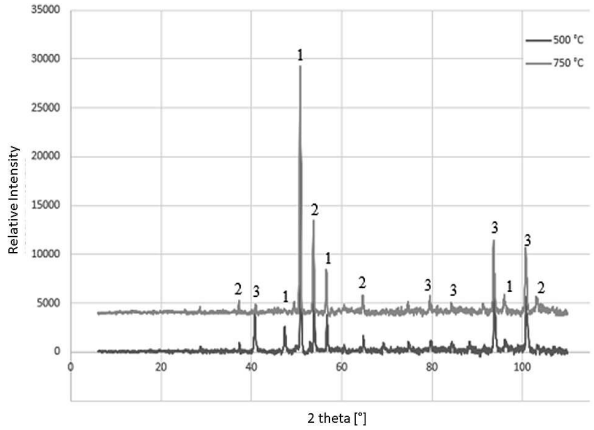


***Fig. 9*** *XRD pattern of the ribbons annealed for 100 h at various temperatures, consisting of phases: 1) β-Mn, 2) $Mn_2FeSi$, 3) $(Cu,Mn)_3(Al,Si)$*

The microstructure of ribbon annealed at 500 °C for 100 h is shown in Fig. 10. The amount of $(Cu,Mn)_3(Al,Si)$ is higher and the darker places corresponding to $Mn_2FeSi$ cannot be distinguished (which is probably dependent on the intensity of etching).

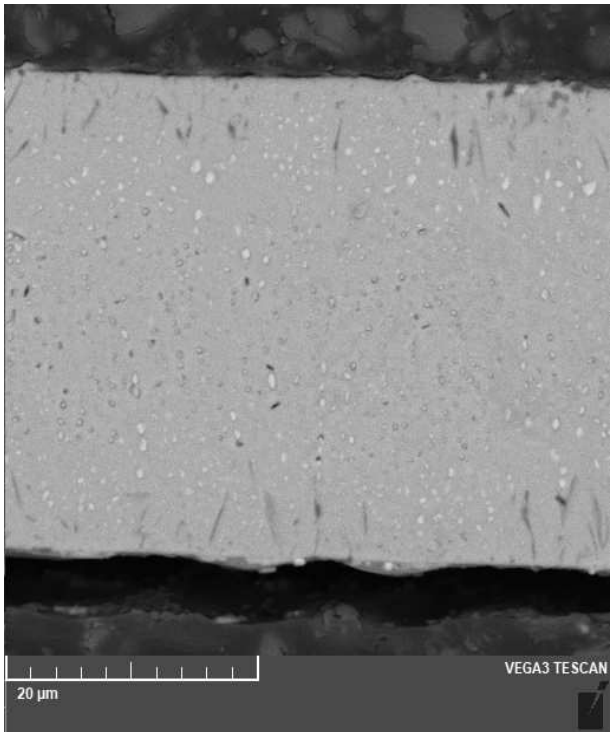


***Fig. 10*** *Microstructure of the ribbon annealed at 500 °C for 100 h (SEM)*

Fig. 11 shows microstructure of the ribbon annealed at 750 °C for 100 h. The areas of $(Cu,Mn)_3(Al,Si)$ phase are significantly larger but no other change can be observe.

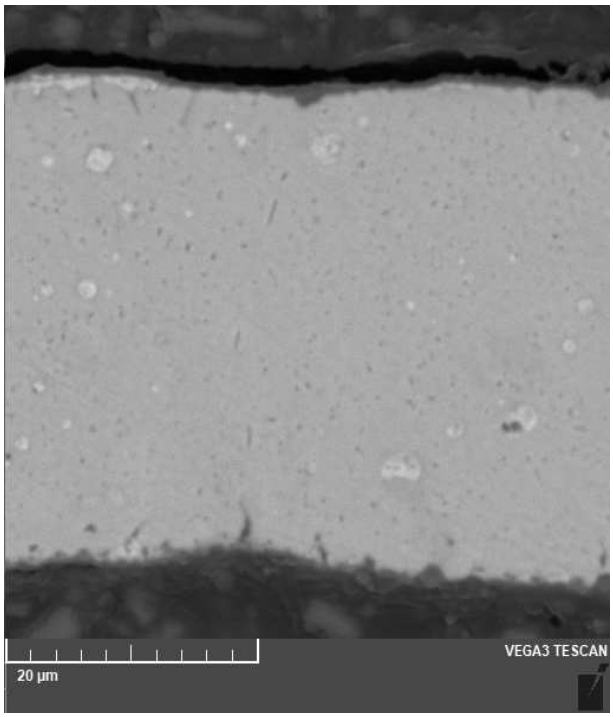


***Fig. 11*** *Microstructure of the ribbon annealed at 750 °C for 100 h (SEM)*

Mechanical properties of the ribbons in the rapidly solidified state and after annealing were characterized by measuring of Vickers hardness HV0.1, see Fig. 12. At all temperatures short term annealing led to increase of hardness probably caused by precipitation of $(Cu,Mn)_3(Al,Si)$ phase. Consequent relaxation led to slight decrease of the hardness, but it did not drop under the initial value of approx. 800 HV0.1. The structure formed by metastable β-Mn and supersaturated intermetallic phases is surprisingly stable.

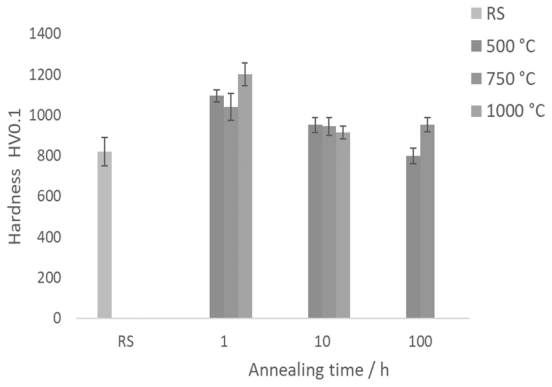


***Fig. 12*** *Dependence of Vickers hardness HV0.1 on annealing time*

Although the conditions for forming the γ-Mn were fulfilled (content of alloying elements, ultrafast quenching), the rapidly solidified ribbons were formed by β-Mn, Heusler phase and intermetallic phase.

## 4 Conclusion

The natural alloy produced by aluminothermic reduction of manganese deep sea nodules (in 20 wt. % excess of Al according to stoichiometry) was successfully processed by melt-spinning. The rapidly solidified ribbons had very fined microstructure and were formed of β-Mn, $Mn_2FeSi$ and $(Cu,Mn)_3(Al,Si)$ (last two probably forming eutectic system). During annealing the microstructure coarsened but the hardness remained high (above 800 HV 0.1) even after annealing at 750 °C for 100 h.

## Acknowledgement

***This research was funded by the Czech Science Foundation (project No. 20-15217S). The authors thank RNDr. Dušan Janičkovič from SAS. Bratislava for processing the melt-spinning process of as-reduced material.***

## References

[1] WANG, X.; MULLER, W.E.G. (2009) Marine biominerals: Perspectives and challenges for polymetallic nodules and crusts. *Trends Biotechnol.* *27*, 375–383, doi:10.1016/j.tibtech.2009.03.004.

[2] RANDHAWA, N.S.; HAIT, J.; JANA, R.K. (2016) A brief overview on manganese nodules processing signifying the detail in the Indian context highlighting the international scenario. *Hydrometallurgy*, *165*, 166–181, doi:10.1016/j.hydromet.2015.09.013.

[3] ZHAO, F.; JIANG, X.; WANG, S.; FENG, L.; LI, D. (2020) The Recovery of Valuable Metals from Ocean Polymetallic Nodules Using Solid-State Metalized Reduction Technology. *Minerals* **2020**, *10*, 20, doi:10.3390/min10010020.

[4] NOVÁK, P.; VU, N.H.; ŠULCOVÁ, L.; KOPEČEK, J.; LAUFEK, F.; TSEPELEVA, A.; DVOŘÁK, P.; MICHALCOVÁ, A. (2021) Structure and Properties of Alloys Obtained by Aluminothermic Reduction of Deep-Sea Nodules. *Materials*, *14*, 561, doi:10.3390/ma14030561.

[5] BORKOVCOVÁ, K.; NOVÁK, P. (2022) Possibilities of a Direct Synthesis of Aluminum Alloys with Elements from Deep-Sea Nodules. *Materials*, *15*, 4467, https://doi.org/10.3390/ma15134467.

[6] BORKOVCOVÁ, K.; NOVÁK, P.; CHMELÍKOVÁ, E.(2022) Processing of Deep-sea Nodules by Silicothermic Reduction. *Manufacturing Technology*, *22(6)*, 655-659, DOI: 10.21062/mft.2022.080.

[7] LEE, H. Y.; HAN, K.H. (1998) Phase constitution and fine microstructure in rapidly solidified austenitic Mn-rich Mn–Al–C alloys. *Journal of Alloys and Compounds*, 281–288, https://doi.org/10.1016/S0925-8388(98)00506-4.

[8] KAWAHARA, K.;. SAKUMA, N.; KIMURA,T. (1989) Workability of manganese-based alloys. *Journal of the Japan Institute of Metals*, *53*, 119 – 125, 10.2320/jinstmet1952.53.1_119.

[9] DUSCHANEK, H.; MOHN, P.; SCHWARZ, K. (1989) Antiferromagnetic and ferromagnetic gamma-manganese generalisation of the fixed-spin-moment method. *Physica B: Condensed Matter.*, *161 (1–3)*, 139–142. doi:10.1016/0921-4526(89)90120-8.

[10] BACON, G E; COWLAM, N A (1970) study of some alloys of gamma -manganese by neutron diffraction. *Journal of Physics C: Solid State Physics.*, *3 (3)*, 675–686. doi:10.1088/0022-3719/3/3/023.

[11] WU, Z.; LIANG, Z.; ZHANG, Y.; LIU, Z.; ZHANG, J.; MOTAZEDIAN, F.; BAKHTIARI,S.; SHARIAT, B. S.; LIU, Y.; REN, Y.; YANG, H. (2019) A eutectic dual-phase design towards superior mechanical properties of heusler-type ferromagnetic shape memory alloys. *Acta Materialia*, *181*, 278-290, https://doi.org/10.1016/j.actamat.2019.09.054.